Correlated errors in geodetic time series: Implications for time-dependent deformation

John Langbein

U.S. Geological Survey, Menlo Park, California

Hadley Johnson

Institute of Geophysics and Planetary Physics, University of California, San Diego, La Jolla

Abstract. Analysis of frequent trilateration observations from the two-color electronic distance measuring networks in California demonstrate that the noise power spectra are dominated by white noise at higher frequencies and power law behavior at lower frequencies. In contrast, Earth scientists typically have assumed that only white noise is present in a geodetic time series, since a combination of infrequent measurements and low precision usually preclude identifying the time-correlated signature in such data. After removing a linear trend from the two-color data, it becomes evident that there are primarily two recognizable types of time-correlated noise present in the residuals. The first type is a seasonal variation in displacement which is probably a result of measuring to shallow surface monuments installed in clayey soil which responds to seasonally occurring rainfall; this noise is significant only for a small fraction of the sites analyzed. The second type of correlated noise becomes evident only after spectral analysis of line length changes and shows a functional relation at long periods between power and frequency of $1/f^\alpha$, where f is frequency and $\alpha \approx 2$. With $\alpha = 2$, this type of correlated noise is termed random-walk noise, and its source is mainly thought to be small random motions of geodetic monuments with respect to the Earth's crust, though other sources are possible. Because the line length changes in the two-color networks are measured at irregular intervals, power spectral techniques cannot reliably estimate the level of $1/f^\alpha$ noise. Rather, we also use here a maximum likelihood estimation technique which assumes that there are only two sources of noise in the residual time series (white noise and random-walk noise) and estimates the amount of each. From this analysis we find that the random-walk noise level averages about 1.3 mm/$\sqrt{yr}$ and that our estimates of the white noise component confirm theoretical limitations of the measurement technique. In addition, the seasonal noise can be as large as 3 mm in amplitude but typically is less than 0.5 mm. Because of the presence of random-walk noise in these time series, modeling and interpretation of the geodetic data must account for this source of error. By way of example we show that estimating the time-varying strain tensor (a form of spatial averaging) from geodetic data having both random-walk and white noise error components results in seemingly significant variations in the rate of strain accumulation; spatial averaging does reduce the size of both noise components but not their relative influence on the resulting strain accumulation model.

Introduction

Although geodetic measurements are a standard geophysical technique to measure crustal deformation, only recently have we begun to appreciate that noise associated with the instability of geodetic monuments can significantly affect the interpretation of these measurements [*Johnson and Wyatt*, 1994; *Johnson and Agnew*, 1995]. The usual assumption is that successive geodetic measurements are statistically independent [e.g., *Agnew*, 1987], which has led some researchers [e.g., *Langbein et al.*, 1982; *Castle et al.*, 1976; *Mark et al.*, 1981] to document time-dependent deformation. In contrast, other attempts to detect possible time-dependent deformation from geodetic data within the San Andreas fault zone in California have

shown only marginally significant changes in deformation rate [*Savage and Lisowski*, 1995a, b, c; *Savage*, 1995]. It is our purpose here to examine high-precision geodetic data to look for possible time dependence of the errors and measure its magnitude. The results demonstrate that the standard assumption of statistical independence for these measurements is not correct. By inference other geodetic measurements will likely demonstrate a component of time-correlated error as well. Any analysis of high-precision data should probably incorporate a time-correlated error of about 1 to 2 mm/$\sqrt{yr}$, reflecting random-walk motion of each geodetic monument.

The results obtained here show that geodetic data are often contaminated by at least two sources of noise: the first being the precision of the instrument and the other being attributed to localized (nontectonic) motion of the geodetic monument. The instrument noise is usually well characterized by both the physical and engineering limitations of the instrument design

and the measurement technique. For traditional electronic distance measuring (EDM) instruments these limitations consist of the measurement of the index of refraction of light averaged over the baseline and the measurement of the travel time of the light beam from one monument to the next. For the Global Positioning System (GPS) data, which are not discussed here, instrument noise includes the phase measurement plus the other variables associated with the data reduction (satellite orbits, troposphere delays, etc.). These noise sources are characterized as being time-invariant but may, in fact, have a time-correlated component as well.

The character of local monument motion appears to have two major components, a seasonal component and a random-walk component. The seasonal component has only been recently recognized in geodetic time series by *Langbein et al.* [1990] because they had frequent and precise enough measurements that showed an obvious 365-day periodicity. Other examples exist, particularly with highly sensitive tiltmeters and strain meters [*Wyatt*, 1982]. Since many geodetic studies of strain accumulation are the result of annual measurements, the effects from seasonal displacements are typically aliased and are not recognized. Some success can be achieved in removing the seasonal fluctuations from the data by using the prior history of rainfall [*Langbein et al.*, 1990], however, a better approach is to improve the stability of the monuments to reduce the contribution from seasonal effects; an example of this has been recently demonstrated by *Langbein et al.* [1995a].

Random-walk noise (also called Brownian motion) in geodetic data is difficult to distinguish from possible variations in the underlying tectonic signals (the geophysical quantity we wish to measure). The most straightforward way to measure the random-walk motion of geodetic monuments would be to make repeated, high-precision measurements in a region that is known to be tectonically stable. In fact, data exist that approach this ideal situation in the form of approximately 15 years of frequent measurements in an area that is only slowly deforming. A network of 12 baselines spans the San Andreas fault at Pearblossom, California (20 km east-southeast of Palmdale), and is measured using an ultraprecise, two-color electronic distance measuring instrument, which we call a two-color EDM. Measurements from this network, and other networks in southern California along the San Andreas fault system, show that strain rates are small (0.2 ppm/yr, or 1.0 mm/yr for a 5-km-long baseline) and that these rates appear to be steady in time [*Savage and Lisowski*, 1995a, c; *Savage*, 1995]. Although further from the concept of zero strain rate, we also analyze data from two additional networks, at Parkfield and Long Valley (Figure 1), where the deformation rate is more than a factor of 10 larger than at Pearblossom. In addition, both surface and borehole strain meter data exist that can be used to place bounds on the amount of noise associated with surface monuments (since the borehole instruments define the upper limit of Earth strain noise [*Johnston*, 1991]).

Many studies of the precision of trilateration and GPS data [*Savage and Prescott*, 1973; *Davis et al.*, 1989; *Larsen and Agnew*, 1991] have equated instrument precision to the standard deviation of residuals about either a mean or secular trend. As we will show below, these estimates of precision will likely include time-correlated errors, but because of the combination of infrequent measurements (once per year) and relatively poor instrument precision with respect to the size of the expected time-correlated errors, the time-correlated errors have

not been detected, and their effect has been lumped together with the apparent instrument precision.

In this study, two different methods have been used to demonstrate that the two-color EDM data contain time-correlated sources of noise and that the functional relationship between noise power and frequency is approximately proportional to $1/f^2$. It is our belief that this noise is the result of small cumulative disturbances of geodetic monuments due mainly to interactions between the surface soils and weather. Although the data analyzed here are not sufficient to prove this causative relationship, we believe the weight of evidence points in this direction. Whether or not this is correct, the correlated nature of the data remains, and its effect on parameters estimated from the raw measurements must be considered.

The data include measurements of line length changes made to a variety of geodetic monuments including those consisting of a steel rod driven to refusal at a depth greater than 1.5 m, tablets glued to outcrop, and a newly designed monument that is braced and anchored to approximately 10 m depth [*Langbein et al.*, 1995a]. There is not yet enough data (particularly for the braced monuments) for us to distinguish between the performance of the different types of monuments.

The data analyzed here are very precise measurements of distance made using a two-color EDM whose precision is better than 1 mm for baseline lengths of less than 10 km. Although time series of daily position measurements from GPS exist, as discussed, for example, by *King et al.* [1995], these measurements are currently about a factor of 3 less precise than the two-color measurements, and their time series are relatively short. In the future these GPS data will provide another means to measure monument instabilities. Thus the high precision of the two-color data, due to its inherent precision and relatively short baselines, along with frequent measurements and long history, make this data set best suited to detect and quantify the correlated noise from geodetic monuments.

The first method we use to examine the frequency dependence in the two-color data is the power spectral density (PSD) of line length changes. These PSD are characterized by two major components, a $1/f^\alpha$ component at long periods, where $\alpha \approx 2$, and a frequency-independent component at short periods. The amount of short-period noise (white noise) has been used by *Langbein et al.* [1987] to measure the instrument precision of the two-color EDM. That report covered only 15 months of frequent measurements, which is not long enough to accurately detect the existence of $1/f^\alpha$ noise in the data. There are now over 10 years of frequent measurements for the networks addressed here, which is sufficient to characterize the frequency dependence of the PSDs. However, since the two-color observations are not typically made on a regular schedule, a reliable estimate of the PSD is difficult. None the less, PSDs from many of these line length data demonstrate a power law dependence with $\alpha \approx 2$ at long periods consistent with other highly sensitive crustal deformation data from creep meters [*Langbein et al.*, 1993a] and strain meters and tiltmeters [*Johnston*, 1991; *Wyatt*, 1982, 1989].

Our second analysis technique assumes a priori that the noise in the data is characterized by a combination of random-walk noise and white noise and then uses a maximum likelihood estimator (M estimate) [*Press et al.*, 1986] to determine the amount of each. This is accomplished by specifying a data covariance matrix containing both the instrument precision and random-walk noise levels and then computing the likelihood function from the data. This function is then maximized
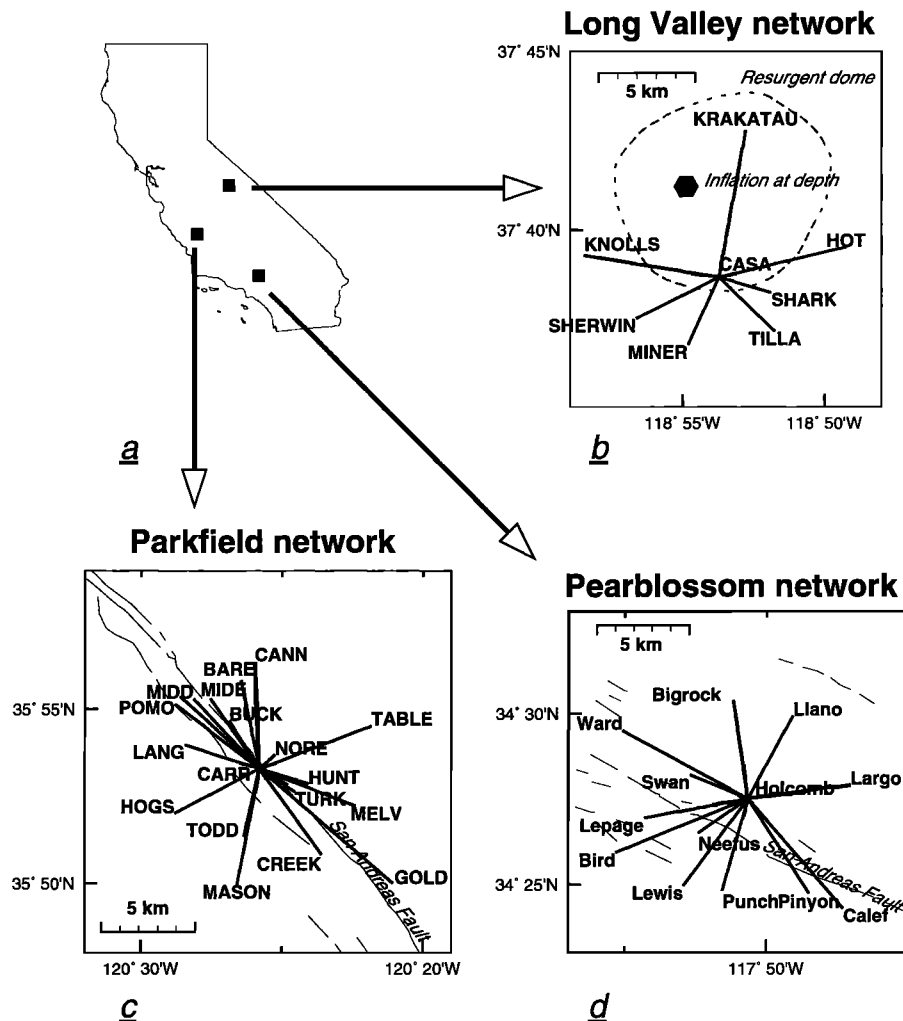
Figure 1. (a) Map of the locations in California of the three geodetic networks used to measure crustal deformation with the two-color electronic distance measuring. (b)–(d) Locations of each baseline within each network.

with respect to both the instrument and the random-walk noise parameters. Importantly, this method does not require regularly sampled observations and overcomes many limitations of the PSD technique.

We first describe the data from the three two-color EDM networks. Then, the power spectral and M estimator techniques are discussed. Both methods are tested with simulated two-color data having known amounts of random-walk noise and white noise. The results of these tests show that the M estimator technique provides accurate estimates for each noise component, and the statistical distribution of the estimates from the simulated data provide a measure of the uncertainty in these estimates. The noise estimates from the power spectral method, however, are not as reliable and are susceptible to problems because of their irregular sampling. In addition, we compare our estimates of random-walk monument noise with other displacement measurements on short baselines of less than 10 m in length, including creep meters and strain meters. Finally, the effect of random-walk noise on estimating strain changes from a suite of baselines will be established.

Data

The line length measurements used here are two-color EDM measurements from three networks in California (Fig-

ure 1): Pearblossom, Parkfield, and Long Valley. Two of these networks, Pearblossom and Parkfield, have been used to measure strain accumulation and slip on the San Andreas fault. The Pearblossom network is located within the "locked" portion of the San Andreas fault and records very little displacement [*Langbein et al.*, 1982]. On the other hand, the Parkfield network is located at the transition of the locked and creeping regions of the San Andreas fault, and accordingly, several baselines show large displacements of about 1 cm/yr because of fault slip [*Langbein et al.*, 1990]. The network at Long Valley responds primarily to deformation from inflation of a caldera that is located just east of Yosemite National Park [*Langbein et al.*, 1993b, 1995b]; several of these baselines show displacements as large as 2.5 cm/yr. Prior to estimating the noise sources in each time series, several preliminary steps are necessary which are summarized below. For all baselines a secular rate and seasonal variation are first removed by least squares fitting of a linear function plus a 365-day sinusoid to the observations. Other parameters, outlined below, are also fit to the data and removed simultaneously with the secular and seasonal components. The seasonal amplitude, which has been previously identified in the Parkfield data by *Langbein et al.* [1990], will be discussed later when it is compared to the random-walk estimates of monument noise.
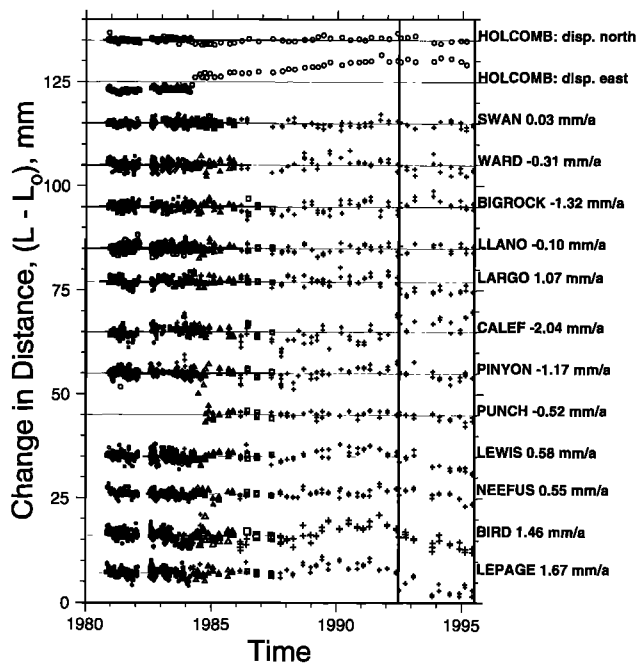
Figure 2. The line length changes for 12 baselines observed at the Pearblossom network. The secular rate of extension has been estimated for each baseline and removed from the data. The estimated secular rate is given next to each baseline. Different symbols designate a change in either the instrument or reflector monument. The vertical line in 1992 represents the time of the Landers, M 7.2 earthquake, located approximately 100 km from the Pearblossom network. In addition, the top two traces show the estimated motion of the central site, Holcomb.

Pearblossom

Line length changes from 15 years of observation with the two-color EDM are shown in Figure 2 for the Pearblossom network. Initially, measurements were made frequently, averaging several times per week for 4 years, but more recently, the sampling frequency has been reduced to once every 3 or 4 months. Because of the infrequent measurements, each baseline is observed at least twice per network occupation to minimize the possibility of blunders in the measurements. For this particular network, three different central monuments at Holcomb have been used over the period of the measurements. Initial measurements, which have been described by *Langbein et al.* [1982, 1987], were made using an observatory-based instrument. Simultaneous measurements of line length were made periodically over 6 months in 1983 using a portable, two-color instrument set up over a second, nearby monument on Holcomb. After the observatory instrument was moved to Parkfield, the portable instrument was used on any of the three monuments on Holcomb. The offset in distance caused by using different monuments is readily constrained using these simultaneous observations. In addition to using different instruments and different monuments, several of the reflector monuments have also changed over time. Fortunately, except for a single case of vandalism at Ward in 1989, there have been simultaneous measurements to neighboring reflector monuments so that the displacement history is kept intact. In addition to the secular motion due to strain accumulation, the only known tectonic signal came from the M 7.2 Landers earthquake in June 1992; these two-color measurements were used

along with other geodetic measurements by *Hudnut et al.* [1994] to model this earthquake. In the end, along with the parameters for the coseismic offset, secular rate, and seasonal amplitude, the offsets from using a variety of instruments and monuments were estimated simultaneously by least squares; this could include as many as a dozen unknown parameters. The standard deviations of the residuals range from 0.7 mm for a 3-km-long baseline to 1.5 mm for an 8-km line. These standard deviations are derived from 15 years of observations and are small by geodetic standards, but they are still a factor of 2 greater than the precision of the two-color technique based upon physical and engineering constraints [*Slater and Huggett*, 1976] and other analyses of the data [*Langbein et al.*, 1987].

Because this network is radial (as are the other two considered in this study), it is possible to estimate the change in position of the central monument as a function of time. This is done by parameterizing the line length change for each baseline into two orthogonal components representing the horizontal displacement of the central monument. Thus the position change of the central monument is relative to the centroid of the network. By using the time-dependent formulation of *Langbein* [1989], the estimate of displacement with time is computed, and this result is shown in Figure 2. The standard deviations of the residual line lengths after adjusting for the displacement of the central monument range between 0.5 mm and 1.4 mm. The residual line length changes will be used in the analysis that follows, as well as the inferred change in position of the central monument. Importantly, since we remove the motion of the central monument from the line length changes, we can assess the noise levels of individual monuments.

The monuments used in this network are a diverse set similar to many geodetic monuments constructed elsewhere. Several monuments, including the three at Holcomb, are tablets that have been glued into outcrop consisting of either limestone, weathered granite, or sandstone. Other monuments consist of cement piers that are trapezoidal in shape and were installed in the 1930s. The remaining monuments consist of galvanized steel pipe (2-cm diameter) driven to refusal at about 1.5 to 2 m depth into granitic alluvium; isolation collars 0.5 m tall minimize the influence of surface soil motion.

Parkfield

At Parkfield there exists over 10 years of line length measurements on 17 baselines which monitor slip and strain accumulation along this reach of the San Andreas fault zone. These measurements have been made approximately 3 times each week. The initial 4 years of measurements have been summarized by *Langbein et al.* [1990], and, at least qualitatively, the character of the recent data remains much the same. The report of *Langbein et al.* [1990] describes several problems with the data which concern the stability of the monuments. Since the reflectors are mounted on the ends of 3-m-long steel pipes (20-cm diameter), for which the lower 2 m have been placed into augered holes, it is possible to periodically measure the tilt of this type of monument, or pier, in terms of the displacement of the top of the pier relative to a point on the pier at ground level. The results of these pier tilt observations are summarized in Table 1 (and Figure 3 of *Langbein et al.* [1990]) in terms of displacement. On a number of these monuments the pier tilt correlates with apparent changes in distances between the reflector and the central instrument monument, Carr. In addition, a few baselines show large, 5-mm seasonal amplitude signal superimposed on a secular trend. *Langbein et al.* [1990]

suggested that these seasonal variations are due to swelling and desiccation of the clayey soil from the seasonal rainfall found in this part of California. In addition, *Langbein et al.* [1990] observed that there was significant, nontectonic motion of the central monument at Carr. Because Carr is located within 100 m of the active, creeping San Andreas fault trace, it is not possible to distinguish the nontectonic, fault-parallel displacement from the signal due to dextral fault slip. However, the fault-normal displacement of Carr is easy to resolve and shows a strong, 2-mm-amplitude seasonal signal.

Data reduction prior to estimating the noise components consists of first removing the secular rate from each baseline. Then, using the residual line length changes from those baselines with small correlation between pier tilt and line length changes (Table 1), the two orthogonal components of motion of the central monument are estimated as a function of time. It is presumed that those baselines with a small correlation ($r <$ 0.5 in Table 1) between tilt and line length are relatively more stable than the other reflector monuments. The line length changes for all baselines are then readjusted for the apparent motion of Carr. Again, the parameters describing the change in position of Carr are also used in the noise analysis. The standard deviations for this reduced data set range between 0.5 mm and 4.3 mm.

Long Valley

In the Long Valley Caldera there are seven baselines with frequent measurements over 11 years starting in early 1984. These measurements, along with other geodetic measurements of deformation of this active caldera, have been recently summarized and modeled by *Langbein et al.* [1993b, 1995b]. As at Parkfield, the measurements of these seven baselines averaged 3 times each week. At two of the sites in Long Valley, pier-type monuments are used which are similar to those at Parkfield. These monuments, which are installed in glacial till, exhibit no obvious correlation between tilt and line length changes (Table 1, Shark and Tilla). The remaining monuments are either tablets glued to volcanic outcrop or large glacial erratics, or the monuments are steel pipe driven to refusal into the glacial till.

Because the rate of inflation of this caldera has not been steady over time, ranging from extension rates of near zero to greater than 40 mm/yr on individual baselines, a model of time-dependent inflation is used to remove the inferred volcanic signal from the data, and the residuals to this model are used for noise analysis. In summary, this model consists of two ellipsoidal sources of inflation described by *Langbein et al.* [1995b], fault slip in the south moat of the caldera described by *Langbein et al.* [1993b] plus motion of the central monument at Casa from the contraction of the crust due to heat extraction used to produce electrical power from the geothermal field near Casa [*Langbein et al.*, 1995b; *Sorey et al.*, 1995]. The standard deviations of the residuals to this model range from 0.8 to 1.4 mm.

Spectral Estimates

Spectral analysis of a time series is the traditional method used to determine the underlying character of the observations provided that the data are sampled at regular intervals and that the number of measurements is large enough so that averaging the PSDs of subsections of the series will result in robust estimates of the power levels. Although the measurements of the three two-color networks span enough time for averaging

Table 1. Correlation of Pier Displacement With Baseline Displacement for Parkfield and Long Valleys

Baseline	Number of Observations	Pier Displacement Rate, mm/yr	Standard Deviation,* mm	Regression of Pier Displacement With Baseline Displacement† Correlation Coefficient	α, mm/mm
Bare	36	0.1	1.35	0.98	3.0 ± 0.1
Mide	46	0.3	0.86	0.93	5.2 ± 0.3
Todd	32	0.1	0.34	0.91	8.8 ± 0.8
Pomo	40	0.1	0.97	0.90	3.8 ± 0.3
Cann	32	0.0	0.30	0.79	3.3 ± 0.5
Table	30	0.1	0.27	0.55	2.5 ± 0.7
Midd	39	0.1	0.36	0.47	2.2 ± 0.7
Hunt	29	0.0	0.16	0.46	1.4 ± 0.5
Creek	30	0.8	1.21	0.37	0.4 ± 0.2
Nore	26	0.0	0.09	0.29	1.9 ± 1.3
Turk	23	0.0	0.16	0.24	0.7 ± 0.6
Buck	26	0.0	0.09	0.20	0.9 ± 0.9
Shark	68	0.1	0.27	0.15	0.3 ± 0.2
Tilla	69	0.0	0.60	0.09	0.1 ± 0.2
Hogs	31	0.2	0.38	0.05	0.1 ± 0.3
Gold	15	0.0	0.20	0.04	0.1 ± 0.9
Lang	27	0.0	0.07	0.01	0.1 ± 2.0
Mason	30	0.0	0.14	0.01	0.1 ± 0.9

*Standard deviation of residual pier displacements about a secular trend.

†Both pier and baseline line length displacements have had secular trends removed prior to regression.

to be effective, the data are not sampled at regular intervals, and substantial gaps exist. If the data gaps are not too long and the sampling rate of the data is fairly constant, interpolation can be used to fill the gaps prior to estimating the PSD. However, simulations of our geodetic data, with their irregular sampling, show that while power spectral techniques can demonstrate the existence of time correlation, they can only provide a rough estimate of the power level of this type of noise.

Where there are gaps in a time series, we average the existing measurements over a 15- to 35-day period spanning the missing datum and use the average as the missing observation. In addition, white noise was added to this interpolate. The amount of white noise is determined by computing the standard deviation of the residuals after fitting a running mean to the entire time series with a window length of between 2 and 4 days. After removing the running mean from the data (which is just a simple form of high-pass filtering), the remaining noise is presumably that caused by the measurement system itself. In fact, the standard deviation of these residuals closely matches the presumed value of instrumental noise characterized as $((0.12 \times 10^{-6} \times L)^2 + 0.3^2)^{0.5}$ by *Langbein et al.* [1987], where L is the nominal baseline length in millimeters.

The power spectrum of each baseline was computed using a window length of 3 years (1100 days) and Hanning tapering [e.g., *Press et al.*, 1986]. The results (see Figure 3 for some examples) show that for longer periods the power density has a $1/f^\alpha$ relation with $\alpha \approx 2$ being a suitable fit. To estimate the size of both the random-walk and white noise components, a curve is fit to the spectral estimates with an equation of the form:
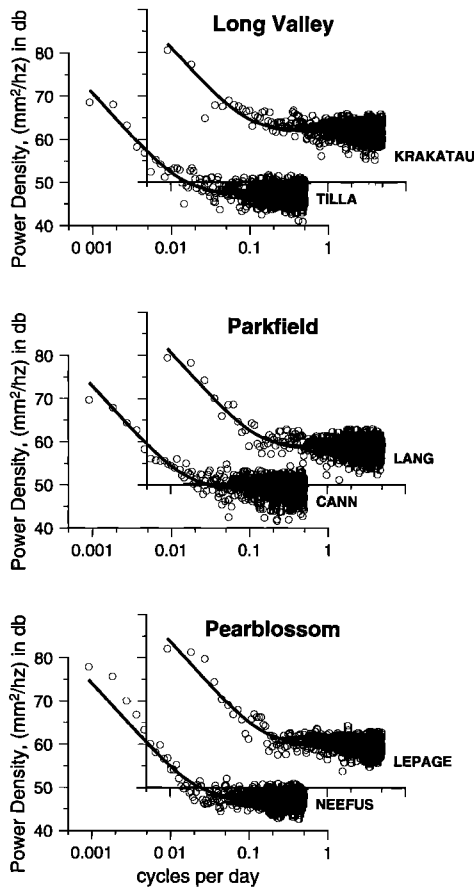
Figure 3. Power spectra and the fitted spectra for a model with a combination of white and random-walk noise are shown for six baselines. The circles are the spectral estimates of power, and the solid curve is the predicted power from the noise model. The 95% confidence limits for the spectral estimates are -3.3 dB and $+5.5$ dB.

$$P(f) = P_0 \frac{[1 + (f/f_0)^\alpha]}{f^\alpha}$$

or in terms of power measured in decibels,

$$10 \log P(f) = 10 \log P_0 + 10 \log [1 + (f/f_0)^\alpha] - 10\alpha \log f$$

where f is frequency and $10 \log P(f)$ is the power density in decibels, and P_0, α, and f_0 are the unknowns to be determined from the fit of the curve to the power spectrum. At long periods, and setting $\alpha = 2$, this curve approaches P_0/f^2 representing the random-walk component, and at short periods the curve approaches a constant, $W_0 = P_0/f_0^2$. Multiplication of W_0 by the Nyquist frequency f_n yields the variance of the white noise σ_w^2 (i.e., $\sigma_w^2 = P_0 f_n/f_0^2$). Similarly, the definition for the random-walk noise is $\sigma_{rw}^2 = 2\pi^2 P_0$ [Agnew, 1992].

Before presenting the results for estimates of the random-walk and white noise parameters, σ_{rw}^2 and σ_w^2, we first simulate the data with known amounts of each noise source to evaluate the accuracy of the estimates. Data from each baseline are simulated by adding two noise time series. The first series is composed of white noise with a standard deviation prescribed by the a priori instrument noise level of $((0.12 \times 10^{-6} \times L)^2 + 0.3^2)^{0.5}$. Next, a random-walk time series is created by integrating white noise having a standard deviation of 1 mm,

with $\delta t = 1$ day and then scaling by $\sigma_{rw}/\sqrt{365}$. After the two series are added together, the synthetic data are sampled on the actual days when two-color measurements were conducted. Using the same process as with the real data, the synthetic data are adjusted for secular motion, offsets, and seasonal variations prior to interpolation and determination of the PSD. Finally, values of P_0, α, and σ_w are estimated from the power spectrum for each baseline of synthetic data. Two or more simulations of each baseline from each network have been made, and the results are summarized in Table 2.

The results in Table 2 are for simulations of three values of σ_{rw}, 0.5, 1.5, and 4.0 mm/$\sqrt{yr}$ and show that the power spectral method does not yield particularly accurate estimates of the random-walk component. However, the method can demonstrate that the simulated data does contain correlated noise since the inferred value of the exponent α is greater than zero and that $\alpha \approx 2$ in many cases. Note that because we remove a secular trend from the synthetic data, as with the real data, this removes significant amounts of low-frequency energy from the time series, and we expect the estimated value of α to be biased to smaller values. In the case where $\alpha = 2$, the estimated values of σ_{rw} are in good agreement when the simulated noise level is 1.5 mm/$\sqrt{yr}$. However, for the simulations with either 0.5 or 4.0 mm/$\sqrt{yr}$, the estimates of σ_{rw} are either biased too high by 50–100% or biased too low by about 30%. Additional tests reveal that these estimates of σ_{rw} are very dependent upon the averaging method used during the interpolation processing.

The estimates for the white noise component (instrumental error) give the expected values as shown in Table 2. It is not surprising that the interpolation processing does not have an effect on these estimates since the interpolated data are drawn from a Gaussian distribution that is based on the a priori instrument error.

M Estimates

Estimating the random-walk and white noise components using the maximum likelihood estimator requires maximizing the probability function by adjusting the data covariance. Thus

$$\text{lik } (\mathbf{x}, C) = \frac{1}{(2\pi)^{n/2}(\det C)^{1/2}} \exp (-0.5\mathbf{x}'C^{-1}\mathbf{x})$$

or

$$\ln [\text{lik } (\mathbf{x}, C)] = -0.5[\ln (\det C) + \mathbf{x}'C^{-1}\mathbf{x} + n \ln (2\pi)]$$

where $\ln$ is the natural logarithm, $\mathbf{x}$ is the data vector, C is the data covariance, n is the number of data, and det is the matrix determinant. The data vector is the same time series used for spectral analysis but without any interpolation since the maximum likelihood estimator (MLE) technique does not require that measurements be made at regular intervals.

We assume that the data covariance matrix is comprised of two parts, a white noise component and a random-walk component. Thus

$$C = \sigma_w^2 I + \sigma_{rw}^2 R$$

where σ_w and σ_{rw} are the magnitude of the white noise and random-walk noise components, respectively, I is the $n \times n$ identity matrix, and R is the matrix representing the covariance of random-walk noise for the data which is scaled by σ_{rw}.

The covariance of random-walk noise is derived from the

Table 2. Spectral Analysis Results From Simulating Two-Color Data

Network	Number of Simulations	Exponent α	Exponent, $\alpha = 2$	
			Random-Walk Noise $\pi\sqrt{2P_0}$, mm/$\sqrt{\text{yr}}$	White Noise Observed/Simulated, mm/mm
For Random-Walk Noise of 0.5 mm/$\sqrt{\text{yr}}$				
Pearblossom	24	1.75 ± 0.41	0.98 ± 0.52	0.95 ± 0.12
Mammoth	14	1.34 ± 0.93	0.84 ± 0.58	0.98 ± 0.07
Parkfield	34	1.29 ± 1.00	0.76 ± 0.50	0.94 ± 0.08
Parkfield and Mammoth	48	1.30 ± 0.99	0.79 ± 0.52	0.95 ± 0.08
For Random-Walk Noise of 1.5 mm/$\sqrt{\text{yr}}$				
Pearblossom	24	1.95 ± 0.22	1.38 ± 0.26	0.95 ± 0.15
Mammoth	14	1.66 ± 0.51	1.34 ± 0.58	0.99 ± 0.11
Parkfield	34	1.53 ± 0.70	1.38 ± 0.35	0.96 ± 0.06
Parkfield and Mammoth	48	1.56 ± 0.65	1.37 ± 0.43	0.97 ± 0.08
For Random-Walk Noise of 4.0 mm/$\sqrt{\text{yr}}$				
Pearblossom	24	2.02 ± 0.18	2.84 ± 1.25	1.21 ± 0.36
Mammoth	14	1.93 ± 0.20	2.67 ± 1.42	1.05 ± 0.12
Parkfield	34	1.90 ± 0.25	2.79 ± 1.28	1.06 ± 0.11
Parkfield and Mammoth	48	1.90 ± 0.24	2.75 ± 1.32	1.05 ± 0.11

process of integrating white noise. Hence, from *Johnson and Wyatt* [1994],

$$R = ZIZ'\delta t$$

where

$$Z = \begin{bmatrix} 0 & 0 & 0 & 0 \\ 0 & 1 & 0 & 0 \\ 0 & 1 & 1 & 0 \\ 0 & 1 & 1 & 1 \end{bmatrix}$$

and where δt is the sampling interval. Here Z is the matrix transformation that integrates white noise into random-walk noise. (Note that the top row and left column of zeros in matrix Z are present to signify that we have no absolute reference frame in which to monitor the random-walk motion. Their effect is to make the first term in the random-walk time series identically zero.) However, if the sampling interval is irregular because of missing data, then the transformation matrix Z is modified to

$$Z = \begin{bmatrix} 1 & 0 & 0 & 0 \\ 0 & 0 & 1 & 0 \\ 0 & 0 & 0 & 1 \end{bmatrix} \begin{bmatrix} 0 & 0 & 0 & 0 \\ 0 & 1 & 0 & 0 \\ 0 & 1 & 1 & 0 \\ 0 & 1 & 1 & 1 \end{bmatrix}$$

where the left-hand matrix samples the data at t_0, t_2, and t_3 in this example. Thus, for the example where data is sampled at day 0, 2, and 3, the covariance matrix is

$$R = \begin{bmatrix} 0 & 0 & 0 \\ 0 & 2 & 2 \\ 0 & 2 & 3 \end{bmatrix} \delta t$$

There are many optimization schemes that can be used to maximize the log likelihood function to find the optimal values of σ_w and σ_{rw}. The only problem arises in the calculation of the matrix determinant of C which can become extremely large or small, of the order of $(\sigma_{rw}^2 T)^n$, for large data sets having n observations and where T is the overall length of the time series in years. This problem is handled by using Cholesky decomposition [e.g., *Press et al.*, 1986] and by removing the average value of the diagonal elements of the decomposed

matrix prior to computing the determinant. The natural logarithm of the average is saved and added to the natural logarithm of the determinant of this modified C matrix.

In addition, since our data vector $\mathbf{x}$ is the residual from a model of secular rate, benchmark swapping, coseismic offsets, and a seasonal cycle, the model coefficients need to be reevaluated with our estimated covariance matrix. Thus the data residuals $\mathbf{x}$ are related to the design matrix A, the model parameters m, and the original data $\mathbf{x}'$ by

$$\mathbf{x} = \mathbf{x}' - Am$$

where

$$m = (A^t C^{-1} A)^{-1} A^{-t} C^{-1} \mathbf{x}'$$

using a least squares formulation [*Menke*, 1984].

The results of computing estimates of the white and random-walk components of noise from synthetic data are summarized in Table 3. The synthetic data have been created by the same method used to test the spectral method in the previous section. The results clearly demonstrate that the M estimator yields an accurate measure of both noise components within the precision shown in Table 3. In contrast, the spectral method yielded significantly biased estimates for data with irregular sampling. Computationally, the M estimator method is considerably slower than the spectral method.

In addition, the M estimator technique is especially sensitive in distinguishing between data that is pure white noise and data that includes time-correlated noise. For instance, using simulated data consisting of only white noise and then estimating the levels of both the white and random-walk components yielded 0.000 ± 0.001 mm/$\sqrt{\text{yr}}$ for the estimate of the random-walk component. Thus the M estimator is a powerful test of the null hypothesis of the data consisting of only white noise.

Multiple simulations of data from one baseline with a specified random-walk noise of 0.5 mm/$\sqrt{\text{yr}}$ and white noise of 0.74 mm indicate that the distribution of the MLE estimates of the noise components is very slightly biased but nonetheless Gaussian about the biased values. Specifically, the distribution of the random-walk component is slightly skewed toward lower values with the mean of the distribution at 0.43 mm/$\sqrt{\text{yr}}$

Table 3. Maximum Likelihood Estimates From Simulating Two-Color Data

Network	Number of Simulations	Random Walk Noise, mm/$\sqrt{yr}$	White Noise (Observed/Simulated), mm/mm	Seasonal Amplitude, mm
		For Random-Walk Noise of 0.5 mm/$\sqrt{yr}$		
Pearblossom	24	0.31 ± 0.30	0.99 ± 0.07	0.18 ± 0.22
Parkfield	34	0.47 ± 0.12	1.00 ± 0.02	0.07 ± 0.08
Mammoth	14	0.49 ± 0.09	0.99 ± 0.03	0.06 ± 0.07
Parkfield and Mammoth	48	0.48 ± 0.11	1.00 ± 0.02	0.06 ± 0.07
		For Random-Walk Noise of 1.5 mm/$\sqrt{yr}$		
Pearblossom	24	1.42 ± 0.30	0.97 ± 0.07	0.29 ± 0.34
Parkfield	34	1.46 ± 0.22	0.99 ± 0.03	0.18 ± 0.21
Mammoth	14	1.70 ± 0.28	0.98 ± 0.03	0.20 ± 0.21
Parkfield and Mammoth	48	1.53 ± 0.24	0.99 ± 0.03	0.19 ± 0.21
		For Random-Walk Noise of 4.0 mm/$\sqrt{yr}$		
Pearblossom	24	4.03 ± 0.45	0.93 ± 0.10	0.67 ± 0.80
Mammoth	14	4.32 ± 0.43	0.93 ± 0.07	0.60 ± 0.66
Parkfield	34	4.13 ± 0.53	0.95 ± 0.09	0.52 ± 0.60
Parkfield and Mammoth	48	4.19 ± 0.50	0.95 ± 0.08	0.54 ± 0.61

(about 15% low). The standard deviation of the distribution about this mean value is 0.11 mm/$\sqrt{yr}$. On the other hand, the distribution of the white noise estimates from the simulated data does not show any systematic bias. As was the case for the spectral estimates, the bias to smaller values of random-walk noise is to be expected because of the fact that we remove significant amounts of energy from the synthetic time series when the secular trend and yearly signals are removed prior to the MLE noise estimation. The estimates of the seasonal amplitude are skewed toward values larger than zero (recall that our simulations have no seasonal cycles as input). This is simply because we have reported only the amplitude of the sea-

sonal cycle and not also its phase. In Table 3 we have been conservative with our estimates of standard deviation of each of the three parameters and use the scatter of the estimates about the specified input value of each parameter.

Results

The results of estimating the size of each component of noise are shown in Figures 4 to 8 along with the 1 standard deviation error bars inferred from the simulations of the two-
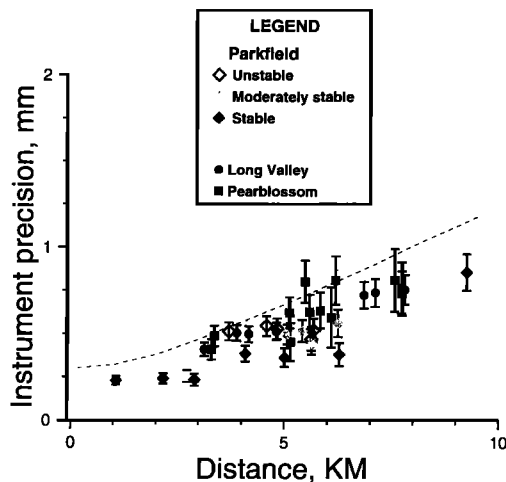

Figure 4. Results of estimating the white noise component of two-color data, which is interpreted to be the instrumental precision, using the spectral approach described in the text. The dashed line is the instrument precision estimated by *Langbein et al.* [1987] and *Langbein* [1989]. The error bars are the result of estimating the white noise component from many sets of synthetic data representing two-color measurements. The estimates for the Parkfield data are designated by three symbols on the basis of the pier displacement measurements in Table 1. Those baselines with high correlation between pier displacements and line length changes are designated as unstable, and those with low correlation are designated as stable.
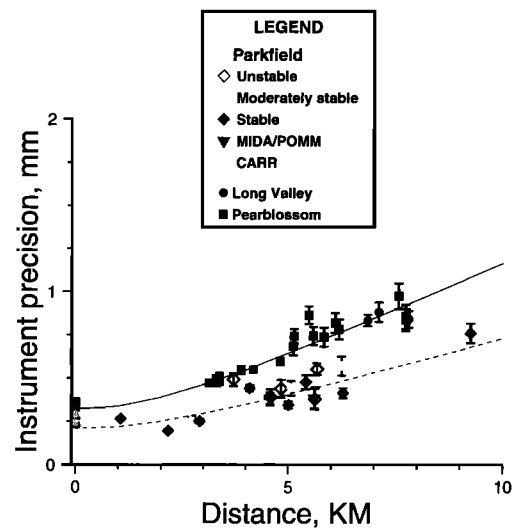
Figure 5. Results of estimating the white noise component of two-color data, which is interpreted to be the instrumental precision, using the M estimator approach described in the text. The solid line is the instrument precision estimated for the measurements of the Pearblossom and Long Valley networks, and the dashed line is the instrument precision estimated for the Parkfield network. The error bars are the result of estimating the white noise component from many sets of synthetic data representing two-color measurements. Included at a distance of zero are the white noise estimates for the inferred, orthogonal components of the central monument displacement data for Pearblossom and Parkfield.
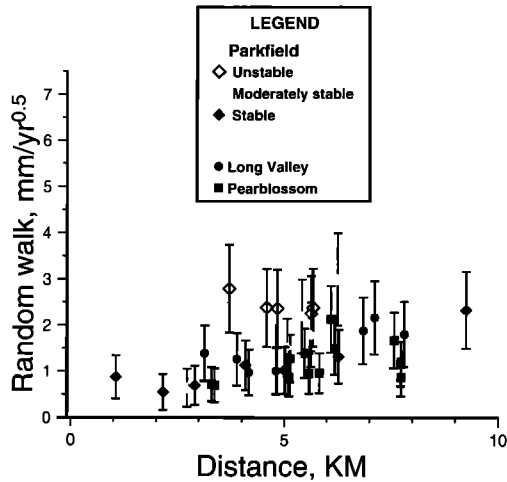
Figure 6. Results of estimating the random-walk component of two-color data using spectral analysis as described in the text. Random-walk noise can be interpreted as local motion of the geodetic monuments. Error bars are the result of estimating the random-walk component from many sets of synthetic data representing two-color measurements. These error bars are the same as those in Table 2.

color data. The two methods, the spectral and the M estimator techniques, yield similar results for the instrument precision, which are shown in Figures 4 and 5. The estimates of random-walk noise, shown in Figures 6 and 7, are qualitatively similar for both methods, but there are some obvious differences
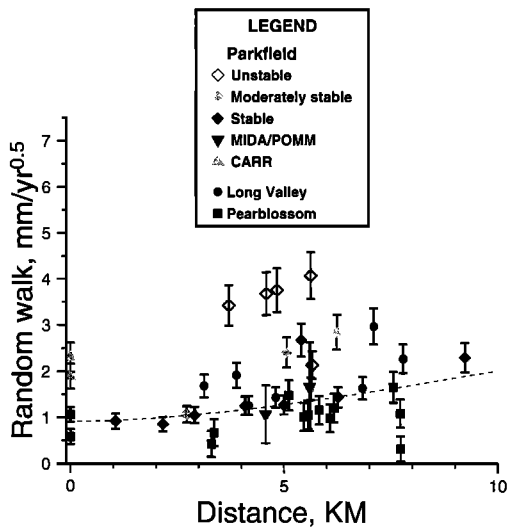

Figure 7. Results of estimating the random-walk component of two-color data using the M estimator method as described in the text. Random-walk noise can be interpreted as local motion of the geodetic monuments. Error bars are the result of estimating the random-walk component from many sets of synthetic data representing two-color measurements. These error bars are the same as those in Table 3. Included at a distance of zero are the random-walk estimates of noise for the inferred, orthogonal components of the central monument displacement data for Pearblossom and Parkfield. The dashed curve is an error model having both length-dependent and length-independent terms that is described in the text. The five unstable baselines from Parkfield were excluded in the derivation of the error model.

which are related to the effects of the interpolation used in the spectral analysis. (Note also that the uncertainties in the error-component estimates are considerably smaller from the MLE technique than from the spectral technique; this can also be seen in Tables 2 and 3.) The relationship between seasonal noise and random-walk noise, computed using the M estimator method, is shown in Figure 8. In addition to the analysis of data from each baseline, the estimates for the noise components for the displacement of the central monuments at Parkfield (Carr) and Pearblossom (Holcomb) are shown for the M estimates corresponding to a baseline distance of zero. Also, the analysis of 2 years of data from two new monuments, Mida and Pomm, at Parkfield [*Langbein et al.*, 1995a] are included in the plot for the M estimates. These monuments are special since they are installed to a depth of 10 m in contrast to the other Parkfield monuments that are installed to a depth of only 2 m; they are located within 30 m of the shallow monuments Mide and Pomo, respectively.

The instrumental noise amplitudes confirm previous estimates of the precision of the two-color EDM, but interestingly, the data from the Parkfield instrument show a better precision than both the Long Valley and Pearblossom data, each of which uses a portable, two-color EDM. The instrument precision can be adequately fit by the relation

$$\sigma_w^2 = (aL)^2 + b^2$$

where L is the baseline length and a and b are the length-proportional and length-independent terms of the error budget for these distance measuring instruments. Fitting this curve to the combination of Pearblossom and Long Valley data yields

$$a = (0.112 \pm 0.006) \times 10^{-6}$$

$$b = 0.32 \pm 0.04 \text{ mm}$$

and for the Parkfield data, the constants are

$$a = (0.070 \pm 0.025) \times 10^{-6}$$
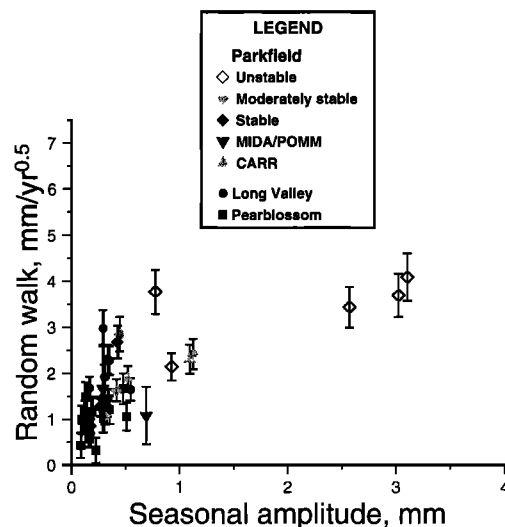
$$b = 0.21 \pm 0.08 \text{ mm}$$

Figure 8. The relation between the inferred seasonal amplitude of baseline displacement and the estimates of random-walk noise using the M estimator.

Table 4. Comparison of Random-Walk Noise Between Shallow and Deeply Anchored Monuments

Monument Pair	Random-Walk Noise, mm/$\sqrt{yr}$	
	Shallow	Deep
Mide/Mida	3.69 ± 0.44	1.08 ± 0.63
Pomo/Pomm	4.08 ± 0.48	1.67 ± 0.96

The above indicates that the Parkfield instrument has better repeatability than the portable instrument which may be partially due to the fact that the Parkfield instrument is never moved, while the portable instruments used at Pearblossom and Mammoth are transported over long distances and generally receive more harsh treatment.

The random-walk error component ranges between about 0.5 and 3.3 mm/$\sqrt{yr}$, with the better monuments averaging about 1.3 mm/$\sqrt{yr}$. The five baselines from Parkfield, Bare, Mide, Todd, Pomo, and Cann, which have been identified as unstable from the high correlation of their pier tilt measurements with changes in distance (Table 1), are clearly the most unstable as identified by both the M estimator and the spectral techniques. In addition, those monuments identified at Parkfield as being relatively stable because of the lack of correlation between their pier tilts and distance changes show fairly low amplitudes of random-walk noise. For one baseline at Pearblossom the random-walk noise could not be reliably estimated for a combination of two reasons: low level of random-walk noise (thus the random-walk component is small relative to the white noise component) and insufficient quantity of data.

The results shown in Figure 7 indicate a possible distance dependence in the estimates of random-walk noise for all baselines excluding the five Parkfield sites previously identified as being unstable. The best fit curve to the random-walk estimates of error is described by the same function used to characterize the instrument error. Thus the coefficients are

$$a = (0.18 \pm 0.09) \times 10^{-6}/\sqrt{yr}$$

$$b = 0.92 \pm 0.43 \text{ mm}/\sqrt{yr}$$

If the length-dependent term is assumed to be zero, then the length-independent term is $b = 1.3 \pm 0.3$ mm/$\sqrt{yr}$, but the increase in the variance of the residuals for this one-parameter model indicates that the length-dependent term is significant at better than a 95% level of confidence.

The source of the length-dependent term is unknown at this time but could be due to unmodeled tectonic processes or to some part of the instrument's error budget that has a time dependence; we do not propose that this length-dependence is due to monument instability. With respect to a time-dependent source in the instrument precision the most likely source is the psychrometer used to measure the partial pressure of water in the atmosphere. For the two-color EDM technique the measurement of the water vapor is the most critical parameter needed to achieve the best precision [*Slater and Huggett*, 1976; *Langbein et al.*, 1987], and possible drift in the thermometers along with changing the psychrometer over time could contribute to the length-dependent term for the random-walk noise.

The correlation between the random-walk noise and the amplitude of seasonal displacement of the baseline data is summarized in Figure 8. The chief observation from this analysis is that those monuments which exhibit a large, seasonal

amplitude tend also to have a large component of random-walk noise. However, the converse is not necessarily true; those monuments with large random-walk components do not always exhibit a large seasonal signal. This behavior can be understood by realizing that the frequency content of a random-walk and a yearly signal overlap and that energy from one noise source can leak into the other during the estimation process. As discussed previously, we remove a several-parameter model from each raw line length time series to produce the residuals which are then analyzed to determine their error structure. One of the components of this model is the yearly signal. If significant energy exists in the time series which is close to, but not exactly at, a 1-year period then it will not be fully modeled by the yearly signal, and energy will remain in the residual series which may then be mistaken for random-walk noise by the MLE routines. In this way it is likely that any time series with significant energy at a yearly period will also exhibit a large random-walk component of noise.

Table 4 compares the random-walk noise for the deeply anchored monuments and their neighboring shallow monuments at Parkfield. These results are particularly interesting since these newer monuments are installed within 30 m of the existing monuments Mide and Pomo, which have shown large, seasonal fluctuations. *Langbein et al.* [1995a] demonstrated that the deeply anchored monuments exhibit about a factor of 5 less seasonal noise than the nearby shallow monuments. In addition to this, Table 4 shows that the random-walk noise is reduced by at least a factor of 3 for the deeply anchored monuments when compared to the neighboring shallow monuments. Taking into account the previous discussion of spectral leakage, we believe this factor of 3 reduction is only a lower bound on the improved stability of the newer monuments. With more data and a more careful removal of energy near a 1-year period, we believe this comparison will demonstrate a larger reduction in the amount of random-walk noise.

Discussion

Comparison With Other Instruments

Creep meter data and their power spectra can be used to help constrain our estimates of monument motion. The creep meter piers at Parkfield are constructed similarly to the two-color EDM piers, but the creep meter piers are located below the ground surface at 1 to 2 m depth and, at least in principle, should be less susceptible to environmental noise. *Langbein et al.* [1993a] examined the creep meter data and computed power spectra for several sites after removing the obvious creep events. Unfortunately, the PSD function of creep data are closer to $f^{-2.5}$ rather than f^{-2}. Taking a representative PSD from *Langbein et al.* [1993a], $P(f) = P_0/f^{-2.5}$, we find that $P_0 = 0.3$ mm yr$^{-0.75}$. From *Agnew* [1992], we find that the root-mean-square variability of the creep data scales as 2.4 mm yr$^{-0.75}$ where, in contrast, the rms variability for the geodetic data scales approximately as 1 mm yr$^{-0.5}$. Thus, in the range between 0.1 year and several years the creep data has at least as much or more variability than the EDM data discussed here.

Another source of displacement data are the strain meters located at both Parkfield and San Juan Bautista, California. Similar to creep meters, these instruments use steel piers that are separated by 10 m and are installed 2 m below the ground's surface. Unlike the creep meters these instruments do not span the active fault trace. These instruments were discussed by *Johnston* [1991] and M. J. S. Johnston (personal communica-

tion, 1995), and the power spectra from their data have been computed. Examination of the amplitude of the f^{-2} part of the spectrum shows that the random-walk noise ranges between 0.1 and 0.2 mm/√yr. These values are better than the surface monuments used with the two-color EDM. In some respects, it is not surprising to see the short-baseline strain meter data show less random-walk noise than the long-baseline EDM data. With a 10-m separation between piers and a 2 m depth of installation these piers experience many random movements in common since they sample nearly the same crustal volume that is of the order of a few tens of cubic meters in size; had the piers been separated by a greater distance, the common mode random movements would become decorrelated, and the apparent random-walk noise of the monuments would increase. This suggests that there is a spatial correlation between geodetic monuments; a component which is not quantified here.

To summarize, it appears that surface monuments installed using traditional geodetic techniques have a random-walk component that is greater than about 0.5 mm/√yr and may be as large as 3 mm/√yr. The length dependence of the random-walk component found in the two-color observations may be due to a previously unknown noise source in the two-color technique, or, as with the creep data, some long-period tectonic signal may be present.

Effect of Monument Noise on Estimates of Strain Changes

Geodetic data are often used to construct models of surface deformation. The presence of time-correlated noise within the data will be propagated through the model, but the level of the noise that is reflected in the estimates of the model parameters will depend upon the amount of spatial averaging that is inherent in the model. One such model, used as an illustrative example, is to compute the changes in tensor strain as a function of time. Figure 9 shows the result of computing these strain changes for the Pearblossom network and from synthetic Pearblossom data using random-walk noise for the central monument of 0.8 mm/√yr and the values of random-walk and white noise for each baseline discussed above. Qualitatively, these time series of strain changes are very similar.

The degree to which random-walk monument motion affects strain change estimates can be determined as follows: At Pearblossom the average length of the 12 baselines is 5 km. Using the functions that characterize both the random-walk and white noise components, the nominal levels of noise for each baseline, expressed in terms of strain, are 0.26 ppm/√yr of random-walk noise and 0.12 ppm of white noise. Since there are 12 baselines from which five components are estimated (three for strain and two for monument displacement), only 7 degrees of freedom remain. If we assume that the errors from one baseline to the next are independent, a reasonable assumption for this approximate calculation, then the overall strain-noise levels for the network should be about √7 times smaller or approximately 0.10 ppm/√yr of random-walk noise and 0.05 ppm of white noise. For comparison, the values of random-walk noise and white noise estimated for the tensor strain changes from the Pearblossom data range between 0.10 and 0.15 ppm/√yr of random-walk noise and between 0.05 and 0.09 ppm of white noise. Within a factor of 2 the amount of estimated strain noise is the same as that determined from actual data.
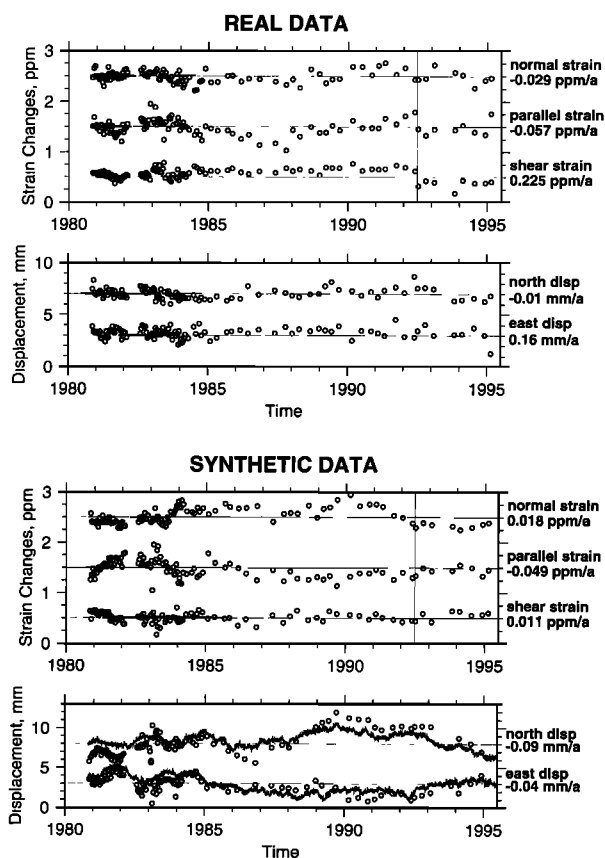

Figure 9. Estimate of the strain changes computed from line length changes at the Pearblossom network using both real data from Figure 2 and synthetic data. (a) Both the components of the displacement of the central monument at Holcomb and the changes in strain are computed as a function of time. The changes have had their secular rates removed, and those rates are shown adjacent to each time series. The vertical line in 1992 corresponds to the time of the Landers M 7.2 earthquake located approximately 100 km east of Pearblossom. (b) Line length changes have been simulated using a combination of white noise, and random-walk noise with a length-dependent amplitude of 0.18 ppm/√yr and length-independent amplitude of 0.92 mm/√yr plus random-walk noise of the central monument of 0.8 mm/√yr. Using this error model, the uncertainty in the estimates of secular strain rate is 0.027 ppm/yr, and the uncertainty in the rate of displacement is 0.27 mm/yr.

Cross-Over Frequency

Time-correlated noise caused by the instability of geodetic monuments has not been an overriding concern for most existing geodetic data sets because of their relatively low sampling rate and relatively large measurement uncertainties. It is easiest to demonstrate this by comparing the theoretical power spectra for random-walk and white noise. The power as a function of frequency for a random-walk process is

$$P_{rw}(f) = \sigma_{rw}^2 / 2\pi^2 f^2 c_1$$

where c_1 is a constant equal to the number of seconds in 1 year ($c_1 = 3.156 \times 10^7$); this clearly shows the expected inverse frequency-squared relationship. The power for a white noise process is

$$P_w(f) = 2\sigma_w^2/f_s$$

where f_s is the sampling frequency in hertz; this power level is independent of frequency. If we define the cross-over frequency as the point at which the power levels of these two processes are equal, we get

$$f_0 = \frac{\sigma_{rw}}{\sigma_w} \frac{1}{2\pi} \sqrt{\frac{f_s}{c_1}}$$

From this equation it becomes clear why most older geodetic data sets have not been able to "see" the long-term correlations discussed in this paper and why the combination of small measurement uncertainty and high sampling frequency are important. Finally, for a time series to be able to accurately characterize the long-period random-walk component, it is necessary, in our experience, to have a length of data of the order of $5/f_0$.

Other than the two-color EDM, the most precise geodetic data come from either Geodolite measurements [*Savage and Prescott*, 1973] or more recently from GPS [*King et al.*, 1995]; the best precision for the former is about 3 mm, while GPS measurements are now approaching 1- to 2-mm precision [*Heflin et al.*, 1995]. Typically, measurements of the Geodolite networks were made about once per year. If we assume a level of monument noise of 1 mm/$\sqrt{yr}$ (toward the low end of what we find for the two-color networks), an instrument precision of 3 mm, and a sampling frequency of once per year, the cross-over frequency is 0.053 cycles per year. Thus a span of approximately 94 years of Geodolite data would be required in order to accurately measure this random-walk component. *Savage and Lisowski* [1995a, b] have reported on Geodolite observations made on an approximately monthly basis. For this data the cross-over period is 5.4 years, and the amount of data needed would be approximately 27 years. More recently, *King et al.* [1995] have reported on daily GPS observations with an instrument error of about 3 mm; the cross-over period is about 1 year, and therefore 5 years of data are required to accurately resolve a random-walk noise of 1 mm/$\sqrt{yr}$. Other GPS studies have reported daily repeatabilities as low as 1 mm [*Heflin et al.*, 1995], and this appears to be about the lower limit of the technique (Y. Bock, personal communication, 1996). Daily GPS observations of this precision would result in a cross-over period of about one third of a year and will require a little over 1.5 years of observations in order to quantify a random-walk error of 1 mm/$\sqrt{yr}$. Finally, the two-color EDM observations analyzed here have a precision of about 0.7 mm and were made at an approximately 3-day sampling interval on the most intensively monitored lines at Parkfield. This combination of values results in a cross-over period of about 5 months, and so about 2 years of data is necessary to characterize a 1 mm/$\sqrt{yr}$ random-walk signal. This study discusses 10 years of frequent two-color observations that have clearly resolved a time-correlated source of noise in the measurements which we attribute, at least in part, to localized motions of the geodetic monuments. High-precision, daily GPS measurements, which were initiated in the last few years, are only now becoming capable of quantifying this random-walk noise.

Other Covariance Models

We have assumed in this study that the low-frequency character of the noise power spectra of the two-color EDM data is best described by a random-walk process. There are, of course,

a large number of other potential models for time-correlated noise, some of which include flicker noise which has a PSD proportional to $1/f$, a first-order Gauss-Markov process which has a PSD proportional to $1/(f^2 + \beta^2)$, and combinations of these with random-walk and white noise models. Each of these noise processes would affect the interpretation of deformation data differently, especially as regards the precision of deformation-rate estimates. At this time it is our belief that the random-walk noise model best characterizes the long-period fluctuations that occur in two-color trilateration data, strain meter data, and presumably GPS data.

Examination of the PSDs in Figure 3, along with the other spectra from the two-color data not shown, suggests that flicker noise does not adequately characterize the frequency-dependent part of these PSDs. The exponent of the long-period part of the PSDs has been estimated and is greater than 1 in all cases which is inconsistent with the theoretical PSD for a flicker noise process.

The PSD of a first-order Gauss-Markov process is random-walk at high frequencies and becomes frequency independent (white) at low frequencies. Such a roll-off at long-periods may be suggested by the PSDs of Figure 3, although we again note that the estimates of the PSD at the lowest frequencies are quite unreliable and will be biased to lower values because we remove a secular trend from the data. This apparent bias is confirmed from simulations of random-walk noise where the PSDs are estimated with and without removing the mean and secular trend from the simulated data. For the PSD computed after removing the mean and secular rate from the data, the estimate of power density at the lowest frequency averages about 9 dB below the spectral estimate from the data for which the mean and secular rate have not been removed.

Given any noise model and its covariance matrix, one may employ the maximum likelihood method to estimate the noise parameters as we have done in this study for the model of random-walk and white noise. Given several noise models for the data covariance and the parameters that optimize each model, one may compare the probability that one model is better than an other. This is a topic for future research, although we also note that the preponderance of evidence from continuous strain meter measurements as well as other geodetic data suggests that the random-walk model best satisfies the observations.

Conclusions

Ultrahigh-precision geodetic data from more than 10 years of measurements from three two-color EDM networks in California have been analyzed to quantify the noise characteristics of the data. Even though the rms deviations of the data for most of the baselines are small, between 0.5 mm and 1.5 mm, this residual noise is still composed of both time-dependent and time-independent components. The time-independent part of the error is characterized by white noise and is about equal to the precision of the instrument used to acquire the data. From spectral analysis the time-dependent part of the noise has an approximate inverse-squared relation between power and frequency, which is as expected for a random-walk process. Comparison of the amplitude of random-walk noise determined from the two-color data with other sensitive crustal deformation instruments implies that most of the source of this noise is likely to be Brownian motion of the geodetic monuments with respect to the deep, stable part of the crust, though

we cannot prove that this is the case. The nominal amplitude of this noise ranges between 0.5 and 2 mm/$\sqrt{yr}$ for most monuments. Some monuments are especially noisy, with random-walk noise as large as 3 mm/$\sqrt{yr}$, and in most cases these can also be identified by large, greater than 2-mm amplitude, seasonal variations. In the data presented here, we also detect a small contribution of random-walk noise that is length-dependent and is likely due to time-correlated error within the instrument system. The correlated nature of this random-walk noise can cause time-dependent fluctuations in a data series which could be misinterpreted as tectonic signals.

References

Agnew, D. C., On noise levels in deformation measurements: Comparison in the frequency domain, *U.S. Geol. Surv. Open File Rep., 87-591*, 839–844, 1987.

Agnew, D. C., The time-domain behavior of power-law noises, *Geophys. Res. Lett., 19*, 333–336, 1992.

Castle, R. O., J. P. Church, and M. R. Elliot, Aseismic uplift in southern California, *Science, 192*, 251–253, 1976.

Davis, J. L., W. H. Prescott, J. L. Svarc, and K. J. Wendt, Assessment of Global Position System measurements for studies of crustal deformation, *J. Geophys. Res., 94*, 13,635–13,650, 1989.

Heflin, M. B., K. J. Hurst, D. C. Jefferson, M. M. Watkins, F. W. Webb, and J. F. Zumberge, Performance of GPS time series in southern California, 1995 (abstract), *Eos Trans. AGU, 76*(46), Fall Meet. Suppl., F141, 1995.

Hudnut, K. W., et al., Co-seismic displacement of the 1992 Landers Earthquake sequence, *Bull. Seismol. Soc. Am., 84*, 625–645, 1994.

Johnson, H. O., and D. C. Agnew, Monument motion and measurements of crustal velocities, *Geophys. Res. Lett., 22*, 2905–2908, 1995.

Johnson, H. O., and F. K. Wyatt, Geodetic network design for fault-mechanics studies, *Manuscr. Geod., 19*, 309–323, 1994.

Johnston, M. J. S. Earth strain noise from deep boreholes near the San Andreas fault system from 0.01 seconds to 100 megaseconds (abstract), *Eos Trans. AGU, 72*(44), Fall Meet. Suppl., p. 484, 1991.

King, N. E., J. L. Svarc, E. B. Fogleman, W. K. Gross, K. W. Clark, G. D. Hamilton, C. H. Stifler, and J. M. Sutton, Continuous GPS observations across the Hayward fault, California, 1991–1994, *J. Geophys. Res., 100*, 20,271–20,283, 1995.

Langbein, J., The deformation of the Long Valley caldera, eastern California, from mid-1983 to mid-1988, measurements using a two-color geodimeter, *J. Geophys. Res., 94*, 3833–3849, 1989.

Langbein, J. O., M. F. Linker, A. McGarr, and L. E. Slater, Observations of strain accumulation across the San Andreas fault near Palmdale, California, with a two-color geodimeter, *Science, 218*, 1217–1219, 1982.

Langbein, J. O., M. F. Linker, A. McGarr, and L. E. Slater, Precision of two-color geodimeter measurements: Results from 15 months of observations, *J. Geophys. Res., 92*, 11,644–11,656, 1987.

Langbein, J. O., R. O. Burford, and L. E. Slater, Variations in fault slip and strain accumulation at Parkfield, California: Initial results using two-color geodimeter measurements, 1984–1988, *J. Geophys. Res., 95*, 2533–2552, 1990.

Langbein, J., K. Breckenridge, and E. Quilty, Sensitivity of crustal deformation instruments to changes in secular rate, *Geophys. Res. Lett., 20*, 85–88, 1993a.

Langbein, J., D. P. Hill, T. N. Parker, and S. K. Wilkinson, An episode of reinflation of Long Valley caldera, eastern California: 1989–1991, *J. Geophys. Res., 98*, 15,851–15,870, 1993b.

Langbein, J., F. Wyatt, H. Johnson, D. Hamann, and P. Zimmer, Improved stability of a deeply anchored geodetic monument for deformation monitoring, *Geophys. Res. Lett., 22*, 3533–3536, 1995a.

Langbein, J., D. Dzurisin, G. Marshall, R. Stein, and J. Rundle, Shallow and peripheral volcanic sources of inflation revealed by modeling two-color geodimeter and leveling data from Long Valley Caldera, California, 1988–1992, *J. Geophys. Res., 100*, 12,487–12,495, 1995b.

Larson, K. M., and D. C. Agnew, Application of the global positioning system to crustal deformation measurements, 1, Precision and accuracy, *J. Geophys. Res., 96*, 16,547–16,566, 1991.

Mark, R. K., J. C. Tinsley, E. B. Newman, T. D. Gilmore, and R. O. Castle, An assessment of the accuracy of geodetic measurements that define the southern California uplift, *J. Geophys. Res., 86*, 2783–2808, 1981.

Menke, W., *Geophysical Data Analysis: Discrete Inverse Theory*, 260 pp., Academic, San Diego, Calif., 1984.

Press, W. H., B. P. Flannery, S. A. Teukolsky, and W. T. Vetterling, *Numerical Recipes, The Art of Scientific Computing*, 818 pp., Cambridge Univ. Press, New York, 1986.

Savage, J. C., Principal component analysis of interseismic deformation in southern California, *J. Geophys. Res., 100*, 12,691–12,701, 1995.

Savage, J. C., and M. Lisowski, Geodetic monitoring of the southern San Andreas fault, California, 1980–1991, *J. Geophys. Res., 100*, 8185–8192, 1995a.

Savage, J. C., and M. Lisowski, Changes in long-term extension rates associated with the Morgan Hill and Loma Prieta earthquakes in California, *Geophys. Res. Lett., 22*, 759–762, 1995b.

Savage, J. C., and M. Lisowski, Interseismic deformation along the San Andreas fault in southern California, *J. Geophys. Res., 100*, 12,703–12,717, 1995c.

Savage, J. C., and W. H. Prescott, Precision of geodolite distance measurements for determining fault movements, *J. Geophys. Res., 78*, 6001–6008, 1973.

Slater, L. E., and G. R. Huggett, A multiwavelength distance-measuring instrument for geophysical experiments, *J. Geophys. Res., 81*, 6299–6304, 1976.

Sorey, M. L., C. D. Farrar, G. A. Marshall, and J. F. Howle, Effects of geothermal development on deformation in Long Valley caldera, eastern California, 1985–1994, *J. Geophys. Res., 100*, 12,475–12,486, 1995.

Wyatt, F., Displacement of surface monuments: Horizontal motion, *J. Geophys. Res., 87*, 979–989, 1982.

Wyatt, F., Displacement of surface monuments: Vertical motion, *J. Geophys. Res., 94*, 1655–1664, 1989.

H. Johnson, Institute of Geophysics and Planetary Physics-0225, University of California, San Diego, 9500 Gilman Drive, La Jolla, CA 92093-0225. (e-mail: johnson@ramsden.ucsd.edu)

J. Langbein, U.S. Geological Survey, MS 977, 345 Middlefield Road, Menlo Park, CA 94025. (e-mail: langbein@shasta.wr.usgs.gov)